Advanced Robotics Research

ADVANCED ROBOTICS RESEARCH Open Access

RESEARCH ARTICLE OPEN ACCESS

Echinoderm-Inspired Autonomy for Soft-Legged Robots

Harmannus A. H. Schomaker[1] | Jelle de Vries[1] | Johannes T. B. overvelde[1,2]

[1]Autonomous Matter Department, AMOLF, Amsterdam, Netherlands | [2]Mechanical Engineering Department, Eindhoven University of Technology, Eindhoven, Netherlands

Correspondence: Johannes T. B. overvelde (overvelde@amolf.nl)

Received: 27 June 2025 | **Revised:** 7 November 2025 | **Accepted:** 4 December 2025

Keywords: bio-inspired | decentralized computation | modular systems | soft robotics | stochastic optimization

ABSTRACT

Soft robots harness their built-in mechanical intelligence to respond directly to their environment. However, they typically still depend on predefined sequences to coordinate their limbs, and external centralized hardware is often used for coordination in changing circumstances. In contrast, in nature, invertebrates like echinoderms distribute behavioral control throughout their body. Inspired by this decentralized computation strategy, we present a modular soft robotic system in which each limb independently adjusts the timing of its actuation to achieve phototaxis via entirely local, stochastic feedback with limited memory. Through this embodied computation approach, coordination emerges from the interaction of the body and the environment. We show robust phototaxis for soft robots that have different morphologies, that undergo damage, and that exhibit highly nonlinear leg behavior, all without an internal body representation. These results, therefore, offer a blueprint for designing resilient, autonomous soft robots that exploit the potential intelligence of their soft adaptive bodies.

1 | Introduction

Living organisms have evolved to exploit mechanical interactions with their environment to achieve function and to delegate computational tasks to their body. Researchers have started to take inspiration from nature to harness such embodied mechanical intelligence (hereafter mechanical intelligence) in the field of soft robotics [1], for example, by developing soft actuators that passively adapt their shape when interacting with their environment. This makes soft devices currently especially suitable for applications that require adaptability, safety, or delicacy [2, 3], such as soft end-effectors for medical and agri-food applications [4].

The mechanical intelligence of soft robots has become a rapidly growing research field. Work in this area has shown how, e.g., underactuated soft grippers can deform to grasp a wide range of objects without changing control input, with compliant materials naturally redistributing forces to accommodate different shapes [5, 6]. In these systems, the control remains fixed while the material adapts [4]. Mechanical intelligence has also been harnessed for locomotion and other behaviors, such as in artificial seeds that dig into soil through humidity-driven deformations, where control emerges from cyclic environmental interactions [7]. Moreover, nonlinear properties such as buckling and snap-through instabilities can be exploited to achieve rapid locomotion or programmed responses to stimuli [8, 9]. Overall, soft robotics has largely followed a bottom-up approach, designing components that exploit material nonlinearities to create new functionalities for predefined scenarios [10–12].

However, integrating these components into multicomponent autonomous systems capable of performing higher-level tasks such as phototaxis remains a challenge. A classical top-down approach that upgrades a central controller to manage all degrees of freedom and nonlinear interactions with the environment quickly becomes intractable [13, 14]. Such models often simplify or neglect nonlinear mechanics to maintain tractability, resulting in reduced embodied intelligence or reliance on external computation [2, 14, 15]. Despite significant progress towards autonomous soft robots, making them untethered, electronics-free, and responsive to environmental cues [16–20], most systems still

depend on preprogrammed behaviors or binary state switching and therefore fall short of autonomously completing more complex tasks. To date, no soft robot has been demonstrated to perform and complete an active search task autonomously with all its decision-making onboard. Hence, there is a need for an alternative approach to autonomy in soft robots that fully embraces the philosophy of embodied computation and mechanical intelligence [1, 21].

The philosophy of soft robotics and its embodied mentality does not end here [1, 21], as nature provides countless examples of achieving autonomous behavior without needing a central brain and using only limited computational power. For example, invertebrates exhibit astounding coordinated behaviors despite missing a skeleton that limits the freedom of motion of their limbs. These creatures utilize what biologists refer to as embodied cognition, which distributes computation from the central brain to other body parts. Besides harnessing their softness, invertebrates employ a localized sensory–motor system to offload computation to their body. For example, an octopus uses its peripheral nervous system to articulate an elbow joint to bring food to its mouth [22, 23], or the camouflage of a catfish, which is largely controlled by organs near the skin [24].

Even though these examples demonstrate the potential of autonomy emerging from embodied cognition, such advanced functionality still seems out of reach. Yet, it does demonstrate key insights that we want to explore further in this work to enable some level of autonomy in soft robotic systems: autonomy does not require full awareness of the body or the environment. In the context of this study, we want to refer to and define three central concepts that together frame our approach. (1) Mechanical intelligence refers to the contribution of a body's intrinsic mechanical properties, such as compliance, nonlinearity, or geometry, to the control and decision-making of the system. (2) Embodied (or distributed) computation describes the process by which local sensing, actuation, and feedback within the body perform the computation required for behavior without relying on a central controller. When these two mechanisms act together to produce adaptive and goal-directed behavior, we refer to this as (3) embodied intelligence, where control emerges from the interaction between the body and the environment.

This concepts play a key role and are particularly clear for lower invertebrates (echinoderms like sea urchins, sea cucumbers, starfish, brittle stars, and feather stars) as they do not have a central brain. Yet, they can navigate a multitude of degrees of freedom and environments to exhibit active foraging behaviors [25]. Echinoderms achieve such behavior through their soft bodies and by performing computations through a minimal radially symmetric nervous system, with a neural ring often centered around the mouth and radial nerves extending to the limbs (depicted in orange in Figure 1a) [26–28].

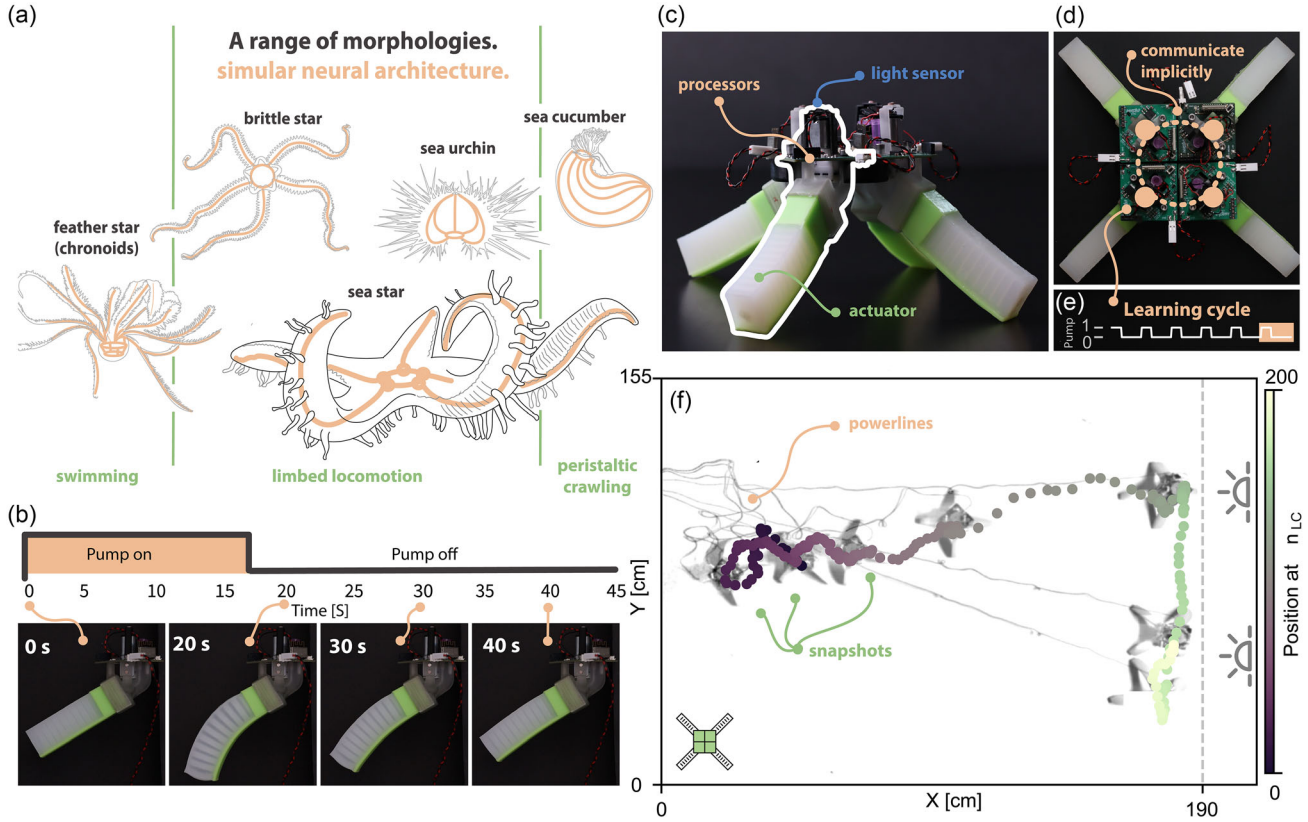

FIGURE 1 | Modular platform inspired by echinoderms to study directed locomotion without a central brain. (a) Echinoderms are classified into five main classes. Directed behavior arises in a range of morphologies from a similar decentralized nervous architecture, highlighted in orange. (b) Cyclic actuation of soft limbs (PneuNet actuators) for the modular platform. (c,d) Each limb of the assembled robot is a self-contained entity capable of actuation, sensing, and computation. (e) Each limb independently undergoes N_{AC} actuations before adapting its behavior. (f) The phototaxis observed for a four-module configuration during 180 learning cycles. The modules are initially positioned on the left with a planar light source on the right side of the image. Black and white background images represent snapshots of the experiment taken every 30 learning cycles.

By using embodied computations that trigger muscle behavior, echinoderms show remarkable adaptation and robustness, both to variations in their environment and to (permanent) changes in their body shape. Even with their limited and distributed nervous systems, echinoderms can perform short-term memory learning [25] and display a wide range of locomotion modalities and behaviors through local action planning and information processing [25]. For example, sea stars, sea urchins, and sea cucumbers utilize similar circular nerve net architectures to achieve different gaits such as peristaltic motion, swimming, and limbed locomotion in various species (Figure 1a) [25, 29–31]. Moreover, similar neural architectures are capable of controlling a diverse range of body plans [32], from worm-like sea cucumbers to limbed brittle stars and spherical sea urchins with hundreds of feet, and even when undergoing damage (Figure 1a) [33, 34]. They also show diversity within species through phenotypic plasticity, where their morphology changes in response to environmental factors and predators [35–37].

In this work, we demonstrate how echinoderm-like autonomy in soft robots can emerge through the direct interplay between embodied computation and mechanical intelligence. We develop a modular soft robotic platform in which each soft limb independently adapts its actuation timing through local sensory feedback and minimal short-term memory. Through this modular platform, we explore how a specific and computationally limited implementation of embodied computation can leverage the existing nonlinear mechanical behavior of soft actuators, that is, their mechanical intelligence, to achieve phototaxis without a central controller. Similar to echinoderms, our implementation of embodied computation results in robust goal-oriented behavior across differently assembled body plans and environments, and even under damage, as demonstrated through a series of experiments. Firstly, by performing experiments with different configurations, we show that the soft robot autonomously finds gaits suited to the changes in the system's morphology. With experiments with damaged systems, we reveal both the limitations and the adaptive capabilities of our approach. Secondly, through experiments with three distinct robotic systems that implement the same embodied computation approach, we demonstrate that the strategy requires neither prior knowledge nor an internal model of the system. Thirdly, by comparing actuators with different mechanical properties across various environments, we show how the mechanical intelligence of the actuators both enables and constrains locomotion. Together, these findings provide insights towards the design of resilient autonomous soft robots that exploit their mechanical intelligence and distributed minimal computation to achieve adaptive behavior (e.g., sequencing) without relying on predefined models.

2 | A Soft Modular Platform to Study Embodied Computations

To study how autonomy can emerge from the interaction between embodied computations and mechanical intelligence, in this work, we focus on an active search task with the aim of having soft robots move toward the area of the highest light intensity (phototaxis). To that end, we introduce modules that each consists of a soft actuator, pneumatic pump, light sensor, and processor (Figure 1c). These modules are assembled in a radially symmetric body (Figure 1d), mimicking the morphology of the echinoderms (Figure 1a). In our implementation, all modules are only mechanically connected, so that there is no explicit communication between them, and computation is fully distributed and embodied. Even though no explicit information is exchanged between the modules, coordination could emerge from the implicitly shared information constituted by their physical connection (Figure 1d). As an example, if the assembled system moves in the direction of the light without rotating, all modules will sense an increase in the light intensity.

Each soft actuator acts as a limb that transforms a cyclic on–off input signal from the pump into a bending motion (Figure 1b). The deformation of the actuator depends both on its design and its interaction with the environment [38], which together define its mechanical intelligence. Additionally, we use the processor to embody computation in each module. We implement an identical algorithm in each module that aims to increase the light intensity measured by the sensors, where we use a basic stochastic updating rule. previously studied in a 1D and 2D framework [39, 40]. In this computationally limited algorithm, the pump oscillates between on and off at a fixed frequency at a specific phase that is kept in the module's short-term memory for six actuation cycles. After these actuation cycles, the module evaluates the difference in the change of the measured light intensity and adapts its phase that is kept in memory accordingly by accepting it or returning to its previous phase. It then randomly perturbs its phase for the next set of actuation cycles. This process is repeated separately in each module, where each complete cycle of evaluating a specific phase is regarded as a learning cycle. We refer to this algorithm's periodic updates as 'learning cycle' as the system as a whole adapts and finds suitable gaits over time. However, it is essential to note the distinction from learning in the classical sense, as the system lacks any form of long-term memory. This process is repeated for N_{LC} learning cycles. The full algorithm can be found in the Supporting Information.

To illustrate the platform, we perform a phototaxis experiment on a flat planar surface where we mount two LED panels on the right side of the rectangular surface (Figure 1f, S1). An assembled robot consisting of four modules is placed on the surface. Note that the assembled system does not have any prior knowledge of its actuator behavior, morphology, and orientation, and starts with random phases. If we then run the experiments for 180 learning cycles, we can observe from Figure 1f that the assembled robot first moves randomly and starts to move away from the light. Yet, at $n_{\mathrm{LC}} \approx 20$, the system reverses its direction to move toward the light. At $n_{\mathrm{LC}} \approx 110$, we see a steep increase in the displacement towards the light, until the system reaches the end of the canvas at $n_{\mathrm{LC}} \approx 135$. Therefore, this initial experiment shows that, in this case, our system learns to coordinate its limbs to achieve phototaxis without a central brain and without explicit communication between the modules. As such, directed behavior at the system level appears in this single experiment to emerge from local sensory feedback without knowing the assembled body plan.

3 | Analyzing the Phototaxis Behavior of a Four-Module Configuration

To understand how the assembled system learns to perform phototaxis, we analyze four different metrics from the single

experiment of the four-module configuration. The first metric is given by the data from the four light sensors inside the modules, and is shown in Figure 2a. These sensors all measure an initial decrease in light intensity (I), followed by only small increases in the light intensity up to $n_{LC} \approx 110$. The following steep increase in light intensity I indicates an apparent behavior switch and increase in performance. Another behavior switch is observed starting from $n_{LC} \approx 130$, where we observe a plateau with only minor fluctuations in I.

However, it is important to note that the modules do not directly use the absolute value of I for their stochastic adaptations. Instead, each module's behavior depends on the difference in light intensity as a result of moving. From this second metric (Figure 2b), we see that ΔI starts negative as the system moves away from the light. It transitions to positive ΔI within $n_{LC} \approx 10$ learning cycles. ΔI slowly increases up to $n_{LC} \approx 122$, where we find the fastest increase. This is followed by a drop in the change in light intensity at $n_{LC} \approx 130$ to around zero as the system reaches the end of the canvas and is not increasing light intensity anymore.

We should mention that the inverse exponential relationship between light intensity and distance means that these results do not reflect the assembled system's actual speed. Therefore, we introduce in Figure 2c the third metric that indicates the global movement speed ΔX of the assembled system (change in X-position per learning cycle). While the overall trend with the individual measured light intensity is the same, we can observe that between $115 \leq n_{LC} \leq 130$ the movement speed of the system reaches a stable maximum of $\Delta X \approx 10$ cm/learning cycle, indicating that it is capable of exploiting stable and relatively fast movement in the direction of the light source.

The observed behaviors are also reflected in the final fourth metric in Figure 2d, which indicates the individual phases of each module throughout the experiment. Initially, for $n_{LC} < 20$, the phase order continually switches as the system explores different gaits. From $20 < n_{LC} < 100$, the front limb (the limb closest to the light source) is actuated first, followed by the other three. Beyond $n_{LC} > 100$, a relatively fast gait emerges where the back limb is actuated later than the center two (Figure 2e–i, Movie S1), a change that drastically influenced the behavior. For $n_{LC} > 130$, the phases start to quickly change again, as the system adapts itself to stop moving to stay close to the light source. These results demonstrate how the system learns to utilize the variable contact friction of its limbs with the ground for locomotion without needing a central brain or a model of its behavior.

To assess the repeatability of this experiment and the learned behavior, we run the experiment five times, each time randomizing the initial phases. The trajectories of all five experiments are depicted in Figure 2j. We found that in four of the experiments, the system learned to move towards the light and reach the

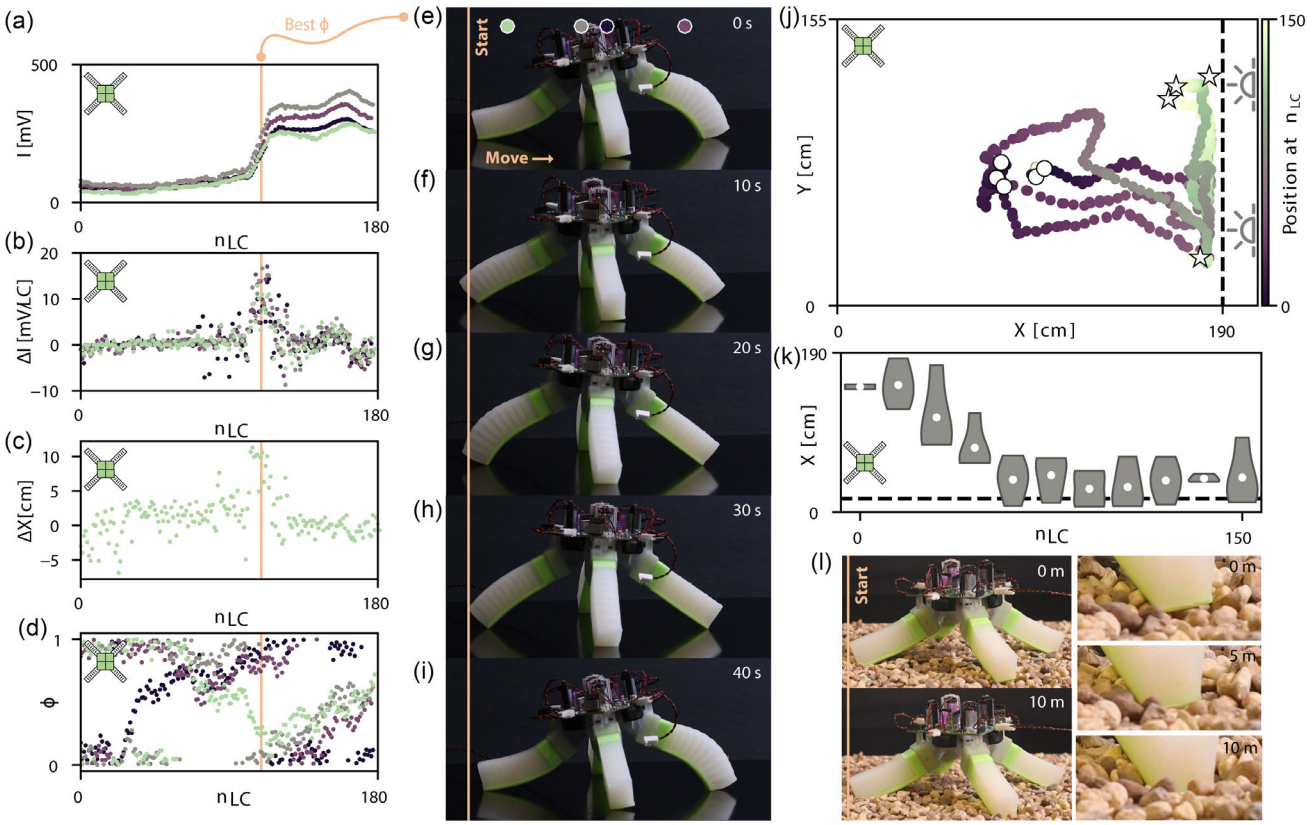

FIGURE 2 | Observed phototaxis behavior of a four-module system. (a) Light measurements, I, from the experiment shown in Figure 1f. (b) Difference in light measurements between learning cycles, ΔI. (c) Displacement of the assembled robot, ΔX, obtained from image tracing. (d) Actuation phases, ϕ_i, for each module. (e–i) Fastest observed phototaxis behavior of the assembled system during the experiment in Figure 1f. (j) Trajectories of five repetitions of the previous experiment, for 150 N_{LC}. Circles and stars indicate the start and end positions, respectively. (k) Distribution of X positions of the system over time during the repeated experiments. The experiment with a broken module at the start of the experiment is excluded from the distributions. This experiment can be found in Figure S2. (l) A similar phototaxis experiment conducted on an irregular surface.

location with maximum intensity (Figure 2k). However, in one experiment, the system did not move (2 cm over 150 learning cycles), which can be attributed to a pump failure at the start of the experiment, resulting in one paralyzed limb (Figure S2).

4 | Robustness Through Embodied Computation

Even though one could consider the experiment in Figure 2j with the paralyzed limb a failed experiment, it underscores an interesting dynamic between embodied computation (learning in the modules) and mechanical intelligence (the mechanical behavior enabled by the assembled soft actuators and their interaction with the environment) that we also find for a three-module configuration in Figure S2e,f: the mechanical behavior of the system influences the ability of the system to achieve goal-directed behavior. Apparently, the potential behavior of a four-module system with only three active legs limits the capabilities of the embodied computation. Similarly, when we place a fully functioning four-module system on a thin layer (2 cm) of gravel (see Figure S2 for a detailed explanation of the setup), we observe that the system is also incapable of moving as it starts to dig itself into the gravel (Figure 2i, Movie S1). In other words, in these scenarios, the system exhibits limited mechanical intelligence as no gait seems to exist that allows it to displace. Hence, the system is not able to find any directed behavior.

In contrast, echinoderms are robust to changes in the environment and body morphologies. For example, researchers have shown that echinoderms can adapt to changes in morphology, such as a reduced number of legs [41]. This points towards introducing redundancy as an aid to increase the potential mechanical behavior that our system can exhibit. Therefore, we begin by increasing the number of modules in the system and changing the body architecture by replacing the type of PLA connectors between the modules (Figure 3). From phototaxis experiments, we find that systems with five and six modules learn to move toward the light in a manner similar to the four-module system (Figure 3a,b).

Interestingly, the fastest observed gaits that emerge for both systems are different (Figure 3d–m). For the five-module system, the two middle limbs inflate, as seen in Figure 3d, followed by the inflation of the two back limbs in Figure 3e, causing the tips of the inflated actuators at the back to creep toward the center of the system. Subsequently, the front limb is actuated to propel the system forward, as it completely lifts the two middle limbs off the ground and causes the back limb tips to stick in place as they deflate. Instead, for the six-module system, we find a gait similar to the four-module system, a propagating wave (Figure 3i–m). Initially, the three back limbs are actuated as seen in Figure 3m, followed by the three front limbs in Figure 3n. Note that we do observe a significant reduction in displacement when comparing the six-module system (≈2.5 cm/cycle) to the

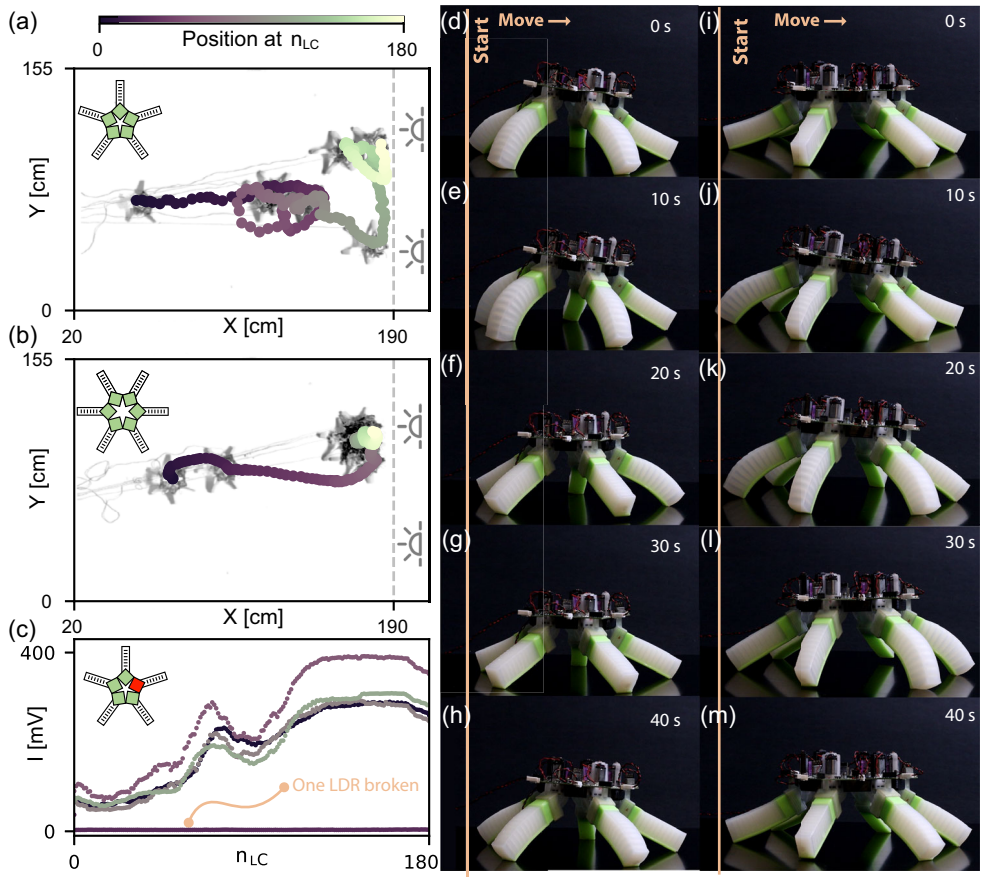

FIGURE 3 | Observed phototaxis behavior of (damaged) five- and six-module configurations. Trajectories of experiments with a (a) five-module configuration, (b) six-module configuration, and (c) five-module configuration with damaged light sensor. Trajectory of the experiment can be found in Figure S3c. (d–h), Fastest observed phototaxis behavior of the assembled system during the experiment in (a). (i–m) Fastest observed phototaxis behavior of the assembled system during the experiment in (b).

five-module system (≈4 cm/cycle), which is likely due to the increased system weight and distance of each actuator to the center of gravity so that it becomes more difficult for each actuator to lift the system.

In addition to these results, which demonstrate how the system harnesses its embodied computation to learn specific gaits that would be challenging to predict and optimize a priori, embodied computation also enables adaptability to unpredictable environmental influences. For example, upon closer inspection of the trajectory of the five-module system (Figure 3a), we observe that at approximately $N_{LC} = 50$, the system briefly loses track of its phototaxis, as it trips over its power line, which causes a relatively quick rotation (Movie S2). Since the system's short-term memory only retains the change in light intensity (and not its orientation), the modules do not directly notice this rotation through their light measurements (Figure S3a). After this interaction, the system adjusts its phases within 50 learning cycles, and redirects its displacement towards the light.

This adaptivity can also be seen in a five-module system where we intentionally damage one of the light sensors, such that it does not give any reading. As shown in Figure 3c and Figure S3c, this damage does not limit the ability of the system to perform phototaxis. Note that the damaged module exhibits random phase changes as a result of the zero light intensity reading, so that the other four modules constantly have to adapt to the damaged module's random behavior (Figure S3d).

5 | Adaptability to Morphological Changes

Based on the evidence of the observed robust behavior in previous experiments, we continue to test the ability of our proposed embodied computation strategy to adapt to morphological variations. We first focus on the six-module system and deliberately simulate damage to change its morphology by removing limbs. Figure 4a illustrates how limbs can be detached, rendering modules without actuators nonoperational. Yet, as the system does not have a central brain, the embodied computation remains functional, such that the remaining modules try to adapt their behavior to the new morphology.

Figure 4b,c demonstrates that even with limbs missing, the system learns to perform phototaxis in two different tested morphologies. Analyzing the emergent behavior can teach us about the interaction between embodied computation and mechanical intelligence. For example, we see that the configuration of Figure 4b is capable of moving in the direction of the light initially. However, the new morphology seems susceptible to rotation, exemplified by the event that occurs around $n_{LC} \approx 150$, where a relatively quick rotation causes the system to enter a dynamic adaptation process that overshoots, causing it to rotate back and forth in a semi-circle. Additional information on these experiments is provided in Figure S4.

Keeping the number of active modules that learn constant (i.e., keeping the computational potential identical), we next explore the system's response to more diverse and heterogeneous

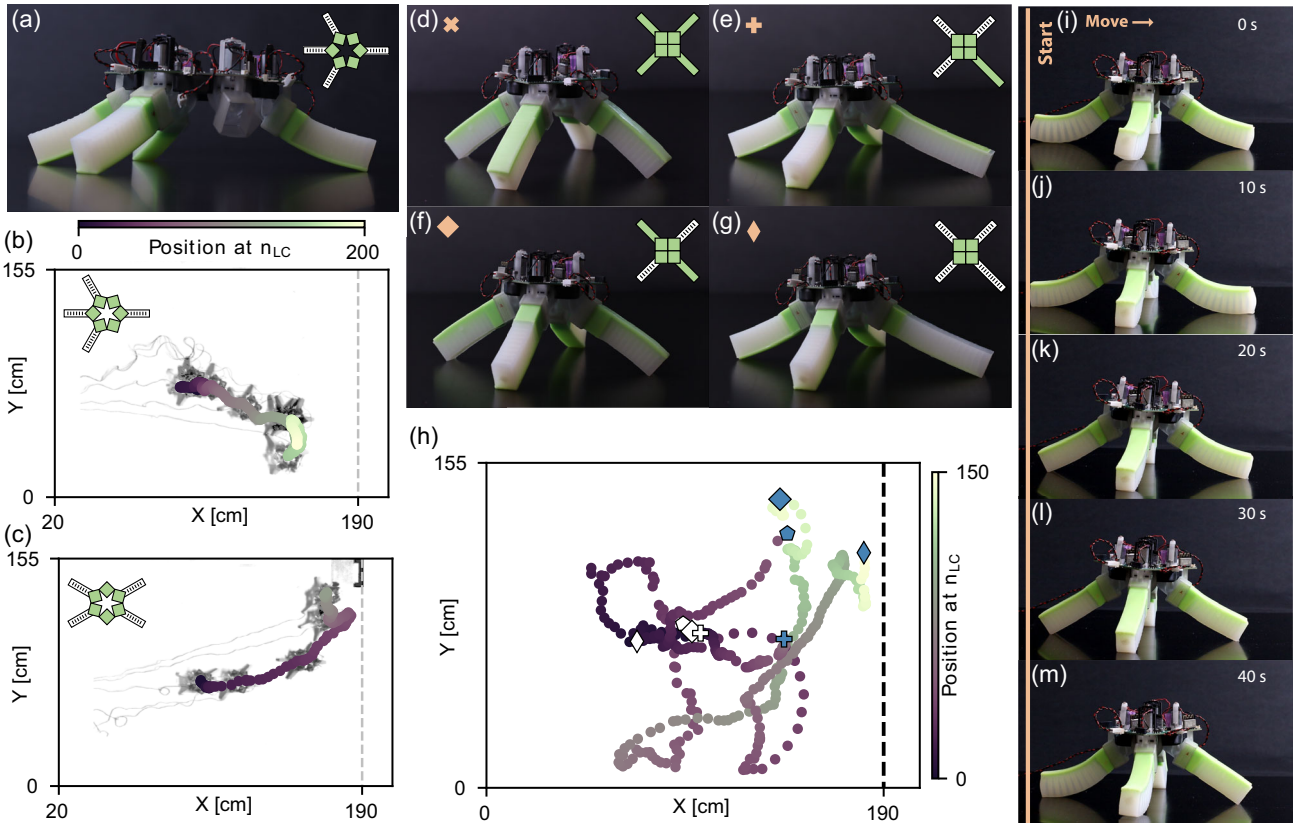

FIGURE 4 | Adaptability of the embodied computation approach to morphological variations. (a) Six-module configuration with two limbs removed. (b,c) Trajectories during phototaxis experiment of 200 N_{LC} for two different configurations. Additional information of the experiment is presented in Figure S4. (d–g) Four different body configurations, including longer and flipped actuators, and (h) the observed trajectories during phototaxis experiments. (i–m) Gait during the best phases of (d).

morphologies. We introduce inverted bending actuators and a longer bending actuator that are 130% of the original length (Figure S5) and establish four distinct body configurations in Figure 4d–g. Figure 4h shows the trajectories of the experiments for these configurations, indicating that all configurations perform phototaxis.

Yet, we also find clear differences between the results of the original four-module configuration shown in Figures 1, 2. Firstly, we find that the configuration with inverted actuators (Figure 4d) is clearly slower than the original configuration, where a gait emerges (Figure 4i–m) that appears to be reversed (back to front propagation of actuation) compared to the gait observed in Figure 2e–i (Movie S3). Secondly, we see that the configurations in Figure 4e,g at some point rotate away from the light source. Similar to the results of Figure 4b,c, these results show that different morphologies can be susceptible to rotation. Lastly, the fastest movement occurs in a configuration where half of the actuators are flipped (Figure 4f), potentially using the additional friction from the flipped actuators as anchor points (details in Figure S5 and Movie S3). Yet, the same morphologies also demonstrate clear and sudden behavior switching as seen by abrupt trajectory changes, indicating more unstable behavior.

By exchanging only the holders and actuators for cubic modules that inflate and deflate, while keeping the same printed circuit boards, light sensors, and pumps (Figure S9a), we demonstrate that the same embodied computation strategy can be directly transferred to a fundamentally different mechanical system (Figure S9b). In this configuration, the cubes can push and pull each other through the inflation and deflation sequence, resulting in a peristaltic-like locomotion pattern (Movie S6). Without modifying the control algorithm, the system harnesses the asymmetry in friction between the cubes and the ground to achieve phototaxis (Figure S9c–g). This generalization highlights that the presented approach is not limited to a specific actuator design or locomotion mode but instead captures a broader principle for achieving autonomous behavior in soft robotic systems with diverse morphologies.

Therefore, these results indicate that even though the embodied computation is capable of handling various morphologies, the emerging behavior that the system shows is the result of the interaction between the embodied computation and mechanical intelligence. Designing soft robots that demonstrate robustness to damage requires redundancy in the design of the system's mechanical intelligence, to which the embodied computation can effectively adapt.

6 | Increasing the Mechanical Intelligence Potential

Changing morphology is not the only way to increase the redundancy embodied in the system. Based on the learned behaviors in the phototaxis experiments performed so far, we find that one of the primary limitations of the PneuNet bending actuators is the reciprocal nature of their inflation-deflation cycle. As a result, several actuators need to interact to enable the friction symmetry to break down at the surface, which is the basis of all the gaits observed so far. Moreover, this also constrains the speed of the system and the variety of terrains it can traverse (Figure 2i). Therefore, we next increase the potential of the mechanical intelligence in each module by leveraging more complex nonlinear behavior in each actuator, allowing it to undergo nonreciprocal (i.e., full-step) motion.

To explore the capabilities of our embodied computation approach, we have developed an actuator that leverages the nonlinear mechanics of thin shells to embed a full-step motion during the inflation and deflation cycles, relying on similar mechanics as [42]. The actuator is shown in Figure 5a, where we show how it goes through four phases during a single actuation cycle. (1) The shell starts fully deflated. (2) The sequence begins with the inflation of the thinner top half of the shell, which pushes a pillar (i.e., the foot that will be in contact with the surface) downward. (3) This is followed by the inflation of the thicker bottom half of the shell that extends the pillar outward. (4) In contrast, during deflation, the circumferential stiffness of the shell maintains the inflated state of the thicker bottom side while the thinner top side deflates. (1) This is concluded with the collapse of the thicker bottom of the shell to reset the actuator to its initial state. The full-step behavior of this actuator can be seen from the hysteresis of the actuator's tip location as depicted in Figure 5b, which clearly differs from the behavior of the PneuNet. As a result of the shell buckling that underlies the hysteretic behavior, we also find that these full-step actuators are more susceptible to interactions with the environment, which complicates feed-forward control without embodied computation (Figure S6b).

Next, the modules are interconnected using the same connectors as previously used to create radially symmetric morphologies. When performing a phototaxis experiment with a four-module configuration, we also observe the phototactic behavior (Figure 5c), where the traveled distance between consecutive learning cycles appears to be significantly increased compared to experiments with PneuNet actuators. Moreover, as expected, the light measurements appear noisier over time, likely due to the actuators' increased stroke and tilting that move the sensors out of plane (Figure 5d). Repeated experiments shown in Figure S6d–h reveal that trajectories vary widely and often appear erratic. Still, in all trials, the system can handle the increased (erratic) movement and achieve movement towards the light source (Figure S6d–h).

The full-step nonlinear motion also opens up the opportunity to traverse more diverse terrains, as the motion is now characterized by the lifting of the limbs instead of the friction-dominated moments we found with the PneuNet actuators. Figure 5e shows how a four-module system comprised of the full-step actuators can learn to achieve phototaxis on an uneven terrain comprising a thin layer of gravel, which was not possible for a four-module system comprised of PneuNet actuators (Figure 2i). All three repetitions of the experiment can be found in Figure S7. When comparing the fastest gait of a four-module assembly of full-step actuators on a flat surface and on gravel, we find a similar gait (Figure 5f,g) in which the system initially lifts off the ground due to inflation of all actuators, after which it propels forward by deflating the two front modules.

These observations underscore the profound synergy between the system's mechanical intelligence and embodied computation, emphasizing that modifications of the body can enhance task performance. Yet, they must not interfere with the predictability of system behavior. Even though phototaxis can still be achieved

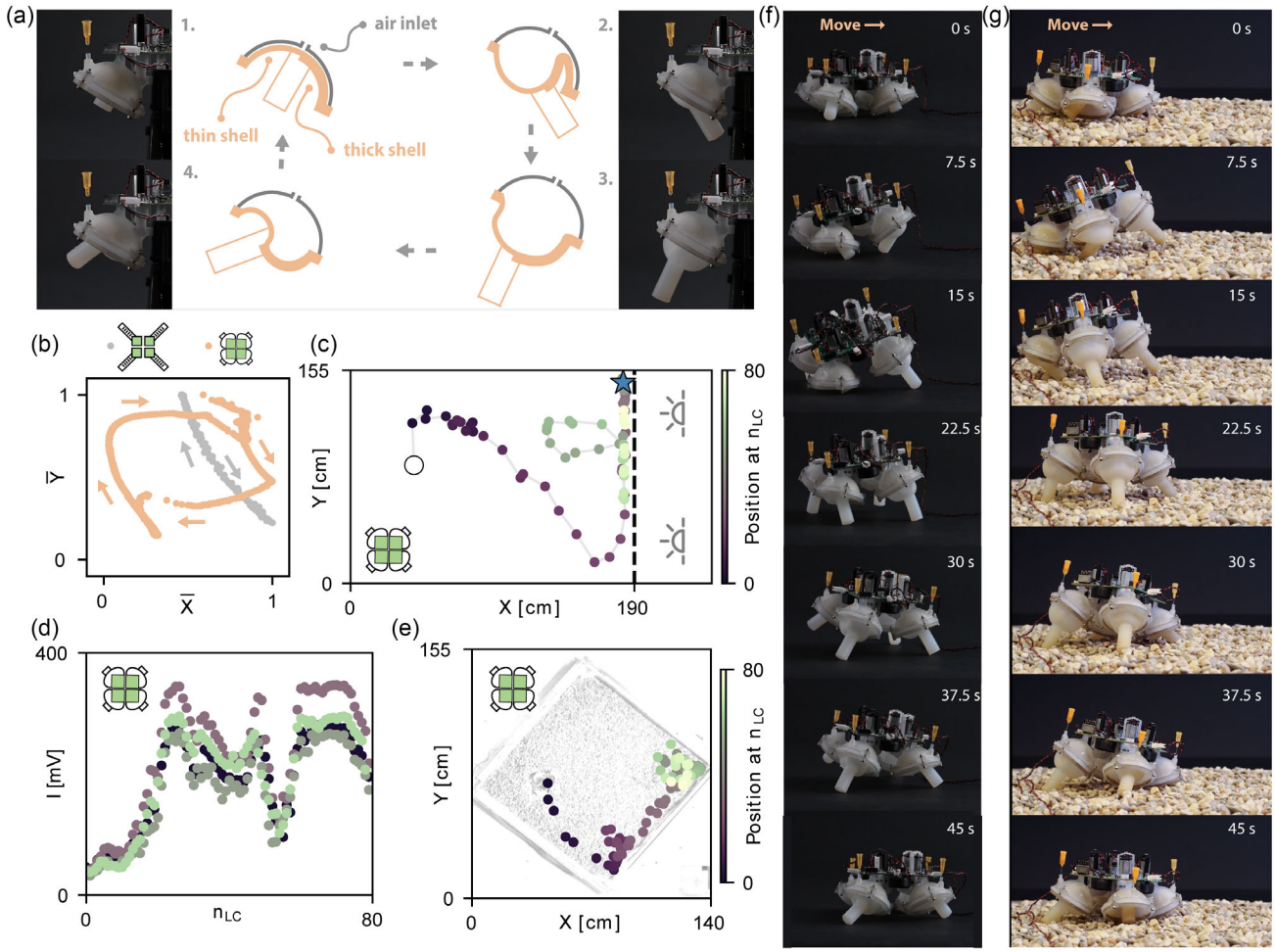

FIGURE 5 | Phototaxis capabilities of four-module systems comprising nonlinear full-step actuators. (a) Experiments and schematic of the inflation-deflation cycle of the "full-step actuator." (b) Reciprocal behavior of the PneuNet actuator and nonreciprocal behavior of the full-step actuator, illustrated by the trajectory of the actuator's tip normalized to the minimum and maximum positions. (c) Trajectory of a phototaxis experiment for a four-module configuration with full-step actuator, for 80 N_{LC}. (d) Light measurements in each module, obtained during the same experiments. (e) The same phototaxis experiment on an irregular gravel surface. More details on the gravel setup are provided in Figure S2. (f) Fastest observed phototaxis behavior during the experiment in (c). (g) Fastest observed phototaxis behavior during the experiment in (e).

for these systems comprising nonlinear and nonreciprocal behavior, current shell actuators seem to push the complexity of the system to its limits, and we expect that at some point, short-term variations become too large for the embodied computation to keep up.

7 | Conclusions

In this work, we demonstrated how 'embodied computation' can leverage the potential of the mechanical intelligence present in soft-limbed robots to achieve a dedicated goal (i.e., phototaxis). In contrast to most approaches to control soft robots that, e.g., depend on predefined or manual sequencing or centralized model representations of the robot's behavior, our developed modular soft robotic platform can achieve emergent directed locomotion without a central brain, a-priory system knowledge, or explicit communication.

We demonstrate that such an embodied computation approach can provide robustness against changes in body morphology, actuator behavior, dynamic environments, or damage. This is illustrated by the various gaits learned in a range of different circumstances (Figures 3d–m, 4i–m, and 5f,g), without requiring any user interference. While we mostly focused on the stochastic adaptation in this work, we believe that our platform can also be used to find gaits for a wide variety of soft robots. As indicated by the three different types of actuators used.

Even though we were inspired by the capabilities of echinoderms that originate from their decentralized architecture, the implementation of the trial-and-error strategy we embodied differs from the exact computations performed by echinoderms. As such, our approach represents only one of many possible implementations of embodied computation. Different fitness functions could give rise to distinct emergent behaviors tailored to various goals. For instance, changing the sign of the measurements might cause the system to move away from the light rather than toward it. Future research could explore alternative formulations and algorithms that may yield different behaviors.

With this approach, we aim to pave the way towards physical implementations that can be realized within the hardware itself. In other words, the minimality of our updating rule is not merely

an abstraction but a critical feature that enables these algorithms to be potentially designed directly into physical materials and mechanical and fluidic interactions [43]. By reducing computational overhead to its bare essentials, we move closer to soft robotic systems whose goal-directed behaviors are inherently embedded and distributed throughout their bodies and actuation physics.

Similar to how natural systems have also co-evolved their body and brain to achieve useful emergent behavior, key in future explorations will be the co-design of both the mechanical intelligence (i.e., body) and embodied computation (i.e., brain). For example, in our system, we observed three instances where the system stopped performing phototaxis. The first two cases are rather obvious, as it seemed to be the result of the system not being capable of locomotion at all, e.g., due to damage as shown in Figure 2k or due to interactions with the environment as shown in Figure 2l. The third case is less obvious and is the result of the interaction between body and brain, where the system got stuck in a dynamic limit cycle due to a delay in sensory observation of the environment (e.g., Figure 4b). Note that in nature, similar unwanted emergent behavior can be observed, such as death spirals in army ants.

We believe that the implications of our research reach beyond the existing platform, promising significant insights on how to incorporate more autonomous behavior in the fields of soft robotics, swarm intelligence, and micro- and nano-robotics [44–46]. The fact that our algorithm is fully decentralized and only requires a few lines of code makes it especially suitable in those applications where computational resources are limited by size, cost, and weight or where behaviors and interactions are difficult or impossible to model a priori. Future research could also explore hierarchical approaches similar to the 'sub-brain architecture' of the octopus and further diversify the tasks the system can perform. As such, we believe our insights on the interaction between embodied computation and mechanical intelligence could lead to a new generation of soft robots that are not only inspired by nature but are also capable of matching its versatility, robustness, and autonomy.

Funding

The authors have nothing to report.

Conflicts of Interest

The authors declare no conflicts of interest.

Data Availability Statement

The data that support the findings of this study are available from the corresponding author upon reasonable request.

References

1. F. Iida and C. Laschi, "Soft Robotics: Challenges and Perspectives," *Procedia Computer Science* 7 (2011): 99–102.

2. G. Mengaldo, F. Renda, S. L. Brunton, et al., "A Concise Guide to Modelling the Physics of Embodied Intelligence in Soft Robotics," *Nature Reviews Physics* 4, no. 9 (2022): 595–610.

3. T. J. Jones, E. Jambon-Puillet, J. Marthelot, and P.-T. Brun, "Bubble Casting Soft Robotics," *Nature* 599, no. 7884 (2021): 229–233.

4. V. G. Kortman, B. Mazzolai, A. Sakes, and J. Jovanova, "Perspectives on Intelligence in Soft Robotics," *Advanced Intelligent Systems* 7, no. 1 (2025): 2400294.

5. E. Brown, N. Rodenberg, J. Amend, et al., "Universal Robotic Gripper Based on the Jamming of Granular Material," *Proceedings of the National Academy of Sciences* 107, no. 44 (2010): 18809–18814.

6. R. Deimel and O. Brock, "A Novel Type of Compliant and Underactuated Robotic Hand for Dexterous Grasping," *The International Journal of Robotics Research* 35, no. 1–3 (2016): 161–185.

7. D. Luo, A. Maheshwari, A. Danielescu, et al., "Autonomous Self-Burying Seed Carriers for Aerial Seeding," *Nature* 614, no. 7948 (2023): 463–470.

8. E. Milana, C. D. Santina, B. Gorissen, and P. Rothemund, "Physical Control: A New Avenue to Achieve Intelligence in Soft Robotics," *Science Robotics* 10, no. 102 (2025): 7660.

9. B. Gorissen, D. Melancon, N. Vasios, M. Torbati, and K. Bertoldi, "Inflatable Soft Jumper Inspired by Shell Snapping," *Science Robotics* 5, no. 42 (2020): 1967.

10. N. El-Atab, R. B. Mishra, F. Al-Modaf, et al., "Soft Actuators for Soft Robotic Applications: A Review," *Advanced Intelligent Systems* 2, no. 10 (2020): 2000128.

11. E. W. Hawkes, C. Majidi, and M. T. Tolley, "Hard Questions for Soft Robotics," *Science Robotics* 6, no. 53 (2024): 6049.

12. J. Walker, T. Zidek, C. Harbel, et al., "Soft Robotics: A Review of Recent Developments of Pneumatic Soft Actuators," *Actuators* 9 (2020): 3, MDPI.

13. F. Tauber, M. Desmulliez, O. Piccin, and A. A. Stokes, "Perspective for Soft Robotics: The Field's past and Future," *Bioinspiration & Biomimetics* 18, no. 3 (2023): 035001.

14. R. Pfeifer, M. Lungarella, and F. Iida, "The Challenges Ahead for Bioinspired 'soft' Robotics," *Communications of the ACM* 55, no. 11 (2012): 76–87.

15. D. Bruder, X. Fu, R. B. Gillespie, C. D. Remy, and R. Vasudevan, "Data-Driven Control of Soft Robots Using Koopman Operator Theory," *IEEE Transactions on Robotics* 37, no. 3 (2020): 948–961.

16. T. TolleyMichael, F. ShepherdRobert, C. GallowayKevin, et al., "A Resilient, Untethered Soft Robot," *Soft Robotics* 1, no. 3, (2014): 213–223.

17. D. Drotman, S. Jadhav, D. Sharp, C. Chan, and M. T. Tolley, "Electronics-Free Pneumatic Circuits for Controlling Soft-Legged Robots," *Science Robotics* 6, no. 51 (2021): 2627.

18. M. Wehner, R. L. Truby, D. J. Fitzgerald, et al., "An Integrated Design and Fabrication Strategy for Entirely Soft, Autonomous Robots," *Nature* 536, no. 7617 (2016): 451–455.

19. W.-K. Lee, D. J. Preston, M. P. Nemitz, et al., "A Buckling-Sheet ring Oscillator for Electronics-Free, Multimodal Locomotion," *Science Robotics* 7, no. 63 (2022): 5812.

20. L. C. Laake, J. Vries, S. M. Kani, and J. T. Overvelde, "A Fluidic Relaxation Oscillator for Reprogrammable Sequential Actuation in Soft Robots," *Matter* 5, no. 9 (2022): 2898–2917.

21. D. Rus and M. T. Tolley, "Design, Fabrication and Control of Soft Robots," *Nature* 521, no. 7553 (2015): 467–475.

22. T. Flash and B. Hochner, "Motor Primitives in Vertebrates and Invertebrates," *Current Opinion in Neurobiology* 15, no. 6 (2005): 660–666.

23. B. Hochner, "An Embodied View of Octopus Neurobiology," *Current Biology* 22, no. 20 (2012): 887–892.

24. C.-C. Chiao, C. Chubb, and R.T. Hanlon, "A Review of Visual Perception Mechanisms that Regulate Rapid Adaptive Camouflage in Cuttlefish," *Journal of Comparative Physiology A* 201 (2015): 933–945.

25. C. A. Freas and K. Cheng, "Neuroecology beyond the Brain: Learning in Echinodermata," *Learning & Behavior* 50, no. 1 (2022): 20–36.

26. K. Cheng, "Cognition beyond Representation: Varieties of Situated Cognition in Animals," *Comparative Cognition & Behavior Reviews* 13 (2018): 1–20.

27. L. Zullo and B. Hochner, "A New Perspective on the Organization of an Invertebrate Brain," *Communicative & Integrative Biology* 4, no. 1 (2011): 26–29.

28. O. Zueva, M. Khoury, T. Heinzeller, D. Mashanova, and V. Mashanov, "The Complex Simplicity of the Brittle Star Nervous System," *Frontiers in Zoology* 15 (2018): 1–26.

29. B. L. Gianasi, J.-F. Hamel, E. M. Montgomery, J. Sun, and A. Mercier, "Current Knowledge on the Biology, Ecology, and Commercial Exploitation of the Sea Cucumber Cucumaria Frondosa," *Reviews in Fisheries Science & Aquaculture* 29, no. 4 (2021): 582–653.

30. H. C. Astley, "Getting around when You're round: Quantitative Analysis of the Locomotion of the Blunt-Spined Brittle Star, Ophiocoma Echinata," *Journal of Experimental Biology* 215, no. 11 (2012): 1923–1929.

31. R. A. Myers, C. M. Furlong, M. K. Gingras, and J.-P. Zonneveld, "Locomotion Traces Emplaced by Modern Stalkless Comatulid Crinoids (featherstars)," *Palaios* 38 (2023): 474–489.

32. L. Formery, P. Peluso, I. Kohnle, et al., "Molecular Evidence of Anteroposterior Patterning in Adult Echinoderms," *Nature* 623, no. 7987 (2023): 555–561.

33. I. Wilkie, "Autotomy as a Prelude to Regeneration in Echinoderms," *Microscopy Research and Technique* 55, no. 6 (2001): 369–396.

34. M. C. Carnevali, "Regeneration in Echinoderms: Repair, Regrowth, Cloning," *Invertebrate Survival Journal* 3, no. 1 (2006): 64–76.

35. A. D. Hughes, L. Brunner, E. J. Cook, M. S. Kelly, and B. Wilson, "*Echinoderms Display Morphological and Behavioural Phenotypic Plasticity in Response to Their Trophic Environment*," *PLoS One* 7 (2012): e41243.

36. T. Ebert, "Adaptive Aspects of Phenotypic Plasticity in Echinoderms," *Oceanologica Acta* 19, no. 3-4 (1996): 347–355.

37. D. K. Barnes and J. D. Allen, "Predators Induce Phenotypic Plasticity in Echinoderms across Life History Stages," *The Biological Bulletin* 244, no. 2 (2023): 103–114.

38. S. Zou, S. Picella, J. Vries, V. G. Kortman, A. Sakes, and J. T. Overvelde, "A Retrofit Sensing Strategy for Soft Fluidic Robots," *Nature Communications* 15, no. 1 (2024): 539.

39. H. Schomaker, S. Picella, A. Küng Garcia, L. Laake, and J. Overvelde, "Robust Phototaxis by Harnessing Implicit Communication in Modular Soft Robotic Systems," *Advanced Functional Materials* 34 (2024): 2310932.

40. G. Oliveri, L. C. Laake, C. Carissimo, C. Miette, and J. T. Overvelde, "Continuous Learning of Emergent Behavior in Robotic Matter," *Proceedings of the National Academy of Sciences* 118, no. 21 (2021): 2017015118.

41. T. Kano, E. Sato, T. Ono, H. Aonuma, Y. Matsuzaka, and A. Ishiguro, "A Brittle Star-Like Robot Capable of Immediately Adapting to Unexpected Physical Damage," *Royal Society Open Science* 4, no. 12 (2017): 171200.

42. M. A. Bell, L. Cattani, B. Gorissen, K. Bertoldi, J. C. Weaver, and R. J. Wood, "*A soft, modular, and bi-stable dome actuator for programmable multi-modal locomotion," in 2020 IEEE/RSJ International Conference on Intelligent Robots and Systems (IROS)* (IEEE, 2020), 6529–6535.

43. S. Picella, C. M. Riet, and J. T. Overvelde, "Pneumatic Coding Blocks Enable Programmability of Electronics-Free Fluidic Soft Robots," *Science Advances* 10, no. 51 (2024): 2433.

44. M. Brambilla, E. Ferrante, M. Birattari, and M. Dorigo, "Swarm Robotics: A Review from the Swarm Engineering Perspective," *Swarm Intelligence* 7 (2013): 1–41.

45. E. Osaba, J. Del Ser, A. Iglesias, and X.-S. Yang, *Soft Computing for Swarm Robotics: New Trends and Applications* (Elsevier, 2020).

46. M. Z. Miskin, A. J. Cortese, K. Dorsey, et al., "Electronically Integrated, Mass-Manufactured, Microscopic Robots," *Nature* 584, no. 7822 (2020): 557–561.

Supporting Information

Additional supporting information can be found online in the Supporting Information section.